Hydrate Formation and Adhesion on Low Surface Energy Materials

by

Taylor A. Farnham

S.B. Mechanical Engineering, Massachusetts Institute of Technology (2014)

Submitted to the Department of Mechanical Engineering
in partial fulfillment of the requirements for the degree of

Master of Science in Mechanical Engineering

at the

MASSACHUSETTS INSTITUTE OF TECHNOLOGY

June 2016

Author .....
Department of Mechanical Engineering
May 18, 2016

Certified by .....
Kripa K. Varanasi
Associate Professor of Mechanical Engineering
Thesis Supervisor

Accepted by .....
Rohan Abeyaratne
Quentin Berg Professor of Mechanics
Chairman, Department Committee on Graduate Theses

Hydrate Formation and Adhesion on Low Surface Energy Materials

by

Taylor A. Farnham

Submitted to the Department of Mechanical Engineering
on May 18, 2016, in partial fulfillment of the
requirements for the degree of
Master of Science in Mechanical Engineering

Abstract

Clathrate hydrates are ice-like solid substances that often form inside oil and gas pipelines and are responsible for flow blockages, sometimes leading to catastrophic disasters. Minimizing hydrate adhesion and accumulation of solids on pipelines can effectively address this problem. In this thesis, we reduce the adhesion of cyclopentane hydrates by promoting the formation of a cyclopentane barrier film between the hydrate and the solid surface. The presence of this liquid film depends on the spreading coefficient of cyclopentane on the solid in the presence of water. Through a systematic modification of the surface chemistry of the solid surface using two different silanes, we correlate the wettability of water and cyclopentane to the adhesion of cyclopentane hydrates. We demonstrate negligible hydrate formation and adhesion on octadecyltrichlorosilane-coated surfaces via macroscopic visualization, surface tilt and adhesion measurements. The use of the spreading coefficient as a design parameter could further advance the development of effective, passive, hydrate-repelling surfaces.

Thesis Supervisor: Kripa K. Varanasi
Title: Associate Professor of Mechanical Engineering

Acknowledgments

I would first like to acknowledge and thank my advisor and thesis supervisor, Prof. Kripa Varanasi, for his numerous insights, academic and professional guidance, and persistent motivation. Without his support, this work would not have been possible.

I would also like to thank the entirety of the members of the Varanasi Research Group, both current and former, for the many discussions, guidance, and assistance over the course of the project. A special thanks to Arindam Das, Srinivas Prasad Bengaluru Subramanyam, and Brian Solomon for their experimental and theoretical expertise and many tangible and intangible contributions. I am further grateful for the insights and comprehensive industrial experience from Uchenna Odi, Alfonso Amendola, and Giuseppe Maddinelli, as well as the funding provided by Eni S.p.A.

Finally, I would like to thank my parents, Stuart and Dianne Farnham, and sister and brother-in-law, Kristen and Brian Reid, for their continued love and support. Their sacrifices and encouragement have enabled all that I have done, and for that I will be forever grateful.

Contents

List of Figures

List of Tables

Chapter 1

Introduction

As world energy consumption continues to rise – the U.S. Energy Information Administration predicts a 56% increase from 2010 to 2040 – a renewed focus will be placed on both expanding current energy sources, and exploring new energy opportunities. [1] This expansion will likely encompass ultra-deep subsea oil and gas exploration and production, which brings a wide array of technical challenges – including the formation of methane hydrates. Methane hydrates, and more broadly clathrate hydrates, are solid, crystalline materials that consist of a cage of hydrogen-bonded water encasing one or more guest molecules. [2] These solids tend to form in areas of high pressure and low temperature, such as deep subsea pipelines, and impede the production of oil and gas. [3] Additionally, as the solids dislodge from the pipe walls they may become pressure-driven projectiles with the potential to damage pipes and equipment – sometimes fatally. [4] Nevertheless, large quantities of methane hydrates exist in shallow waters (above 2000m depth) and currently exceed the known reservoirs of conventional natural gas and may present an economic energy opportunity in the future. [5]

Presently, clathrate hydrates are seen as an impediment to production and considerable efforts are taken to mitigate their formation. These efforts largely consist of: introducing chemical inhibitors to make hydrate formation less favorable or to impede the growth of hydrates, heating and insulating pipe walls to avoid the low temperature formation regime, or relocating wells to avoid hydrate formation

conditions. [3, 6, 7] Many of these approaches are energy-intensive, environmentally-unfriendly, and economically-unfavorable, with costs exceeding $200M USD annually. [8] As such, hydrate accumulation and adhesion is of great interest and has been the focus of several scientific works. [9–18] More recent studies have begun to explore the role of solid surface chemistry on the adhesion of hydrates, including the interfacial tension between hydrate forming agent and water. [10, 13–15, 17] However, the current work seeks to expand this knowledge by considering the three-phase interaction between the hydrate forming agent, water, and the solid substrate in the analogous case of cyclopentane hydrates.

By considering this three-phrase interaction, the current work re-explores the fundamentals of hydrate accumulation and adhesion and provides a new understanding into a potential mechanism for mitigating these effects. This mechanism manifests itself as a thin barrier film of the hydrate forming agent between water and the solid surface. The liquid film then depends on the spreading coefficient of the hydrate forming agent on the solid, in the presence of water. Forming the thin film dramatically reduces the interfacial contact between the water and the solid surface, ultimately resulting in reduced hydrate accumulation and adhesion. The methods and insights shown in this work may be later expanded and deployed to larger industrial-scale applications.

Chapter 2

Experimental Procedures

While methane hydrates are most prevalent in the oil and gas industry, the extreme conditions required for their formation are often prohibitive in the laboratory environment. This study uses cyclopentane hydrates as a model system for the methane hydrates found in pipelines. Cyclopentane hydrates have the same crystalline structure as methane hydrates (SII), and a critical temperature of 7.7°C at ambient pressure. [19] Possessing a critical temperature above the freezing point of water is especially valuable in preventing ice contamination during formation. Three methods for hydrate formation are discussed, but ultimately only results from *Hydrates Formed via Seed Crystal* were reported as that was determined to be most representative of actual conditions.

2.1 Hydrate Formation via Emulsion

Hydrates were first formed from an emulsion of cyclopentane and water. Emulsions of 10:1 cyclopentane to water, and 10:1 water to cyclopentane (by volume) were produced by rigorously sonicating. The sample of interest was then placed at the bottom of a transparent rectangular quartz cuvette and submerged with either emulsion. The cuvette was placed atop a Peltier chiller and chilled to 1°C and a rotary mixer was then introduced to continually agitate the emulsion. After the hydrate was formed the samples were removed from the cuvette and assessed for hydrate accumulation.

In order to avoid the effects of surfactants, and minimize confounding factors, none were added to stabilize the emulsion. As a result, the emulsion required constant agitation to prevent coalescence. While this provided useful dynamic properties, and was later refined into the *Hydrate Accumulation* procedure, it was ill-suited for static experiments.

2.2 Hydrate Formation via Ice Precursor

Hydrates for static experiments were initially formed from initially frozen water droplets submerged in cyclopentane. Test samples were placed at the bottom of a transparent rectangular quartz cuvette and submerged with cyclopentane. The cuvette was placed atop a Peltier chiller and water droplets were dispensed onto the surface. The cuvette was chilled to -20°C and the water droplets were permitted to freeze and were held for 10 minutes. The bath temperature was increased to 1.3°C and held for 60 minutes to permit the ice to melt and nucleate hydrate formation. Finally, the temperature was further increased to 5.4°C and held for 60 minutes to ensure no ice remained in the hydrate crystals. While this enabled hydrate adhesion studies in static cases, the phase change from ice to liquid water, and associated localized heat transfer, deviated too considerably from the original system of interest. This deviation may have adversely affected initial adhesion results and was ultimately replaced by the *Hydrate Formation via Seed Crystal* method.

2.3 Hydrate Formation via Seed Crystal

Hydrates for static experiments were ultimately formed directly from chilled water with the introduction of pre-formed seed crystals. Samples were placed at the bottom of a transparent rectangular quartz cuvette and submerged with cyclopentane. 3μL water droplets were introduced on top of the samples and the cuvette was placed atop a Peltier chiller (Stir-Kool) and chilled to 1°C. Simultaneously, an additional crystal was formed using the *Hydrate Formation via Ice Precursor* method. A small portion

of the ice-formed hydrate was collected with a 100μm diameter steel wire (Hamilton Co.) and was introduced to the tops of the chilled water droplets to initiate hydrate nucleation. The cuvette was held at 1°C for 4 hours prior to conducting adhesion force measurements to permit complete formation of hydrate without introducing ice. This final method permits the study of hydrate formation under static conditions with minimal effects from heat transfer. Additionally, since any potential heat transfer from the needle and ice-formed hydrate occurs at the top of the water droplet, it is less likely to affect hydrate adhesion.

2.4 Surface Texturing

Photolithograph was utilized to impart controlled micro-textures onto the silicon wafers used in this study. The micro-textures of interest consist of 10μm square posts separated by an inter-post spacing of 5, 10, 25, 50, or 75μm. 150mm silicon wafers were first rinsed with acetone and isopropanol until they were free of dust and debris. Shipley 1818 photoresist (Dow Chemical Company) was spun onto the wafers, which were then exposed to a 405nm wavelength ultraviolet light source using a chrome mask (Advance Reproductions Corporation) for the desired texture. The photoresist was developed in a solution (equal parts by volume) of deionized water and Microdev solution (Dow Chemical Company). Once developed, the wafer was etched to a depth of 10μm using an inductively coupled plasma reactor (Surface Technology Systems) and confirmed via surface profilometry with an optical profilometer (CCI HD Optical Profiler, Taylor Hobson). Any remaining photoresist was removed by submersion in piranha solution (3:1 volume ratio of sulfuric acid to hydrogen peroxide).

2.5 Surface Functionalization

For surface functionalization and adhesion measurements, 150mm silicon wafers were cut to 20mm squares to promote uniform coatings and to facilitate handling. A 1064nm Nd:YAG laser (Electrox) was used to score or dice the wafer and any final

cleavage was performed manually. The 20mm samples were then coated with either OTS (octadecyltrichlorosilane, Sigma-Aldrich) or FS (tridecafluoro-1,1,2,2 tetrahydrooctyltrichlorosilane, Sigma Aldrich) through liquid and vapor deposition, respectively.

To deposit OTS, samples were plasma-cleaned for 30 minutes then submerged in a mixture of 75mL toluene and 250μL OTS. Simultaneously, an emulsion of 325μL water (18.2M, Millipore) and 50mL toluene was prepared through 90 seconds of vigorous mixing with a probe sonicator (Sonics 750W). The emulsion was added to the OTS-toluene mixture and the resultant mixture was placed in an ultrasonic bath sonicator (Branson) for 120 seconds. Excess OTS was removed by rinsing with acetone and isopropanol.

To deposit FS, samples were plasma-cleaned for 30 minutes then placed in a vacuum desiccator with 10μL FS. The desiccator was purged to vacuum three times in a sequence of 2, 5, and 2 minutes each. After the third purge the desiccator was sealed under vacuum and held for 4 hours. Excess FS was removed by rinsing with acetone and isopropanol.

2.6 Contact Angle Measurement

Advancing and receding contact angles of various fluid combinations on samples were measured using a Ramé Hart M500 goniometer. The sample was placed at the bottom of a transparent rectangular quartz cuvette and the first, surrounding liquid (either cyclopentane or water) was introduced to submerge the sample. Approximately 50μL of the second liquid (either water or cyclopentane) was then drawn into the goniometer. 5μL drops of this second liquid were dispensed onto and retracted from the sample at a rate of 0.2μL/s while advancing and receding contact angles were measured, respectively. A minimum of ten measurements were performed on each sample; the average and standard deviation are reported.

2.7 Hydrate Accumulation

Hydrate accumulation was assessed under rotary mixing conditions. Samples were placed at the bottom of a transparent rectangular quartz cuvette and submerged in cyclopentane. The cuvette was then placed atop a Peltier chiller (Stir-Kool), which was chilled to -5°C, until it reached a stable temperature and was held for 15 minutes. A mechanical rotor was introduced to the cyclopentane bath and spun at 200rpm. Over 30 seconds, a 36-gauge needle was used to dispense a total of 0.3mL of water in the form of droplets approximately 100μm in diameter. Once the droplets were introduced and free to flow around the cuvette the temperature of the cyclopentane bath was periodically cycled. Varying the temperature between -5°C and 5°C at 1°C/min for 30 minutes allowed for the freezing of the water and the initiation of hydrate nucleation at the ice-cyclopentane interface. The bath temperature was ultimately held at 5°C for an additional 90 minutes to melt any remaining ice without dissociating the hydrate.

2.8 Adhesion Force Measurements

The adhesive force between the sample and hydrate was measured using the deflection of a cantilevered stainless steel wire, similar to methods previously described elsewhere. [9] After the hydrate had fully formed on the surface, the bottom end of a thin wire was brought alongside the hydrate. The top end of the wire was fixed to a micro-manipulator stage and was slowly moved to exert a force on the hydrate until the hydrate adhesively or cohesively fractured. Two configurations of needles were used, as shown in Figure 2-1. While the longer needle enabled measurements with finer resolution for lower adhesion, the shorter needle was necessary to dislodge more strongly adhered hydrates. A DSLR camera (Nikon) with a high-zoom macro lens (Navitar) was used to record a video of the hydrate detachment. Image analysis was used to measure the displacement of the cantilevered wire during the fracture. The adhesion force was calculated from the wire's deflection, material, and geometric

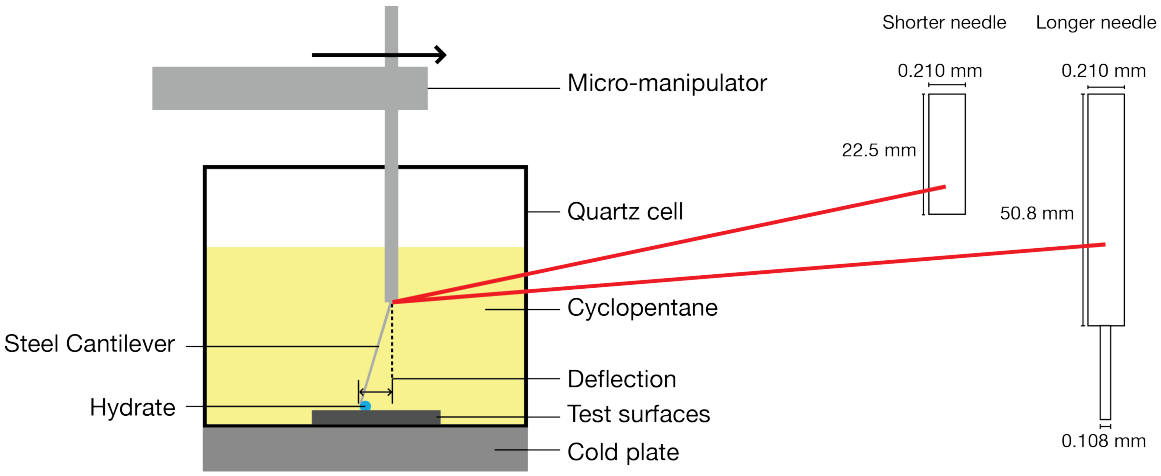

Figure 2-1: (left) Schematic of the adhesion force setup, and (right) dimensions of needles used for deflection.

properties using classical cantilevered beam deflection equations. [9]

Chapter 3

Interfacial Spreading

Figure 3-1 demonstrates cyclopentane hydrate accumulation on substrates with varying surface chemistries at 5°C. As one may expect, the bare silicon surface, with the highest surface energy ($\sim 51\frac{mJ}{m^2}$), shows the highest hydrate accumulation with a combination of large hydrate clusters and a thin layer covering the remaining surface. The two silane-modified surfaces (octadecyltrichlorosilane (OTS) and tridecafluoro-1,1,2,2 tetrahydrooctyl-trichlorosilane (FS)) show substantially less hydrate formation, consistent with their reduced surface energies. However, contrary to conventional wisdom, the FS-coated surface with the lowest surface energy ($\sim 8\frac{mJ}{m^2}$) has a greater coverage of hydrate crystals than the OTS-coated surface with a higher surface energy ($\sim 24\frac{mJ}{m^2}$). [20] The OTS-coated surface appears entirely free of hydrate accumulation and exactly resembles an untested sample.

This unexpected behavior is further studied in terms of the interfacial interactions between the solid substrate, water, and cyclopentane in order to determine the affinity of a hydrate crystal to a substrate. The spreading coefficient is introduced in this work as a more accurate design criterion to account for the influence of these three-phase interfacial interactions on hydrate formation and adhesion.

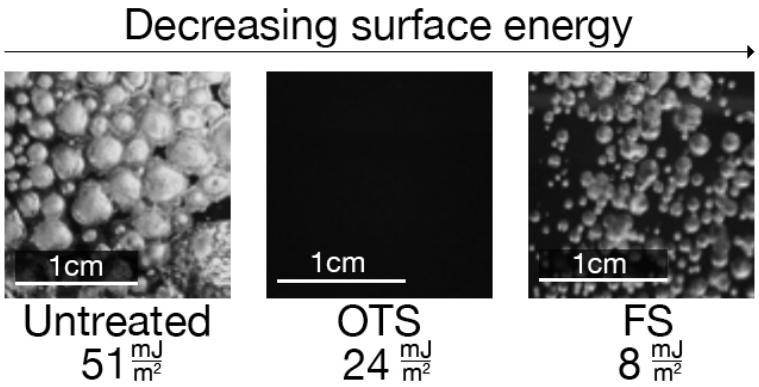

Figure 3-1: Hydrate accumulation on smooth untreated, FS-treated and OTS-treated surfaces

Table 3.1: Dynamic contact angles and roll-off angles of water droplets (3μL) in cyclopentane

	Advancing angle	Receding angle	Contact angle hysteresis	Roll-off angle
Untreated	$78° \pm 4°$	$54° \pm 4°$	$\sim 24°$	$> 90°$ (Sticks)
FS-treated	$153° \pm 4°$	$99° \pm 5°$	$\sim 55°$	$> 90°$ (Sticks)
OTS-treated	$164° \pm 2°$	$163° \pm 2°$	$\sim 1°$	$< 2°$ (Slides)

3.1 Water Contact Angle and Cyclopentane Spreading Coefficient

Water and cyclopentane are the precursors for cyclopentane hydrates and their wettabilities can be used to compare hydrate formation and adhesion on different surfaces. Dynamic contact angles and sliding angles of water on untreated, OTS-treated, and FS-treated silicon surfaces are tabulated in Table 3.1.

The water contact angle hysteresis on the untreated and FS-treated surfaces in cyclopentane is quite high and, as a result, a water droplet sticks to the surface even at a 90° tilt angle. On the OTS-treated surface, however, the water contact angle hysteresis and the roll-off angles in an environment of cyclopentane are much lower, which indicates the presence of a thin film of cyclopentane underneath the water drop. In other words, the spreading coefficient of cyclopentane in water, $S_{os(w)}$, is positive for OTS-treated surfaces and negative for FS-treated and untreated surfaces. The

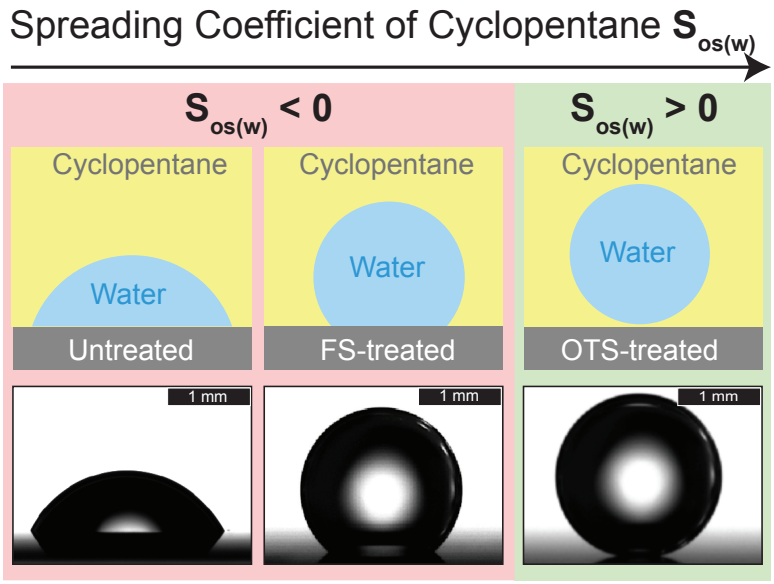

Figure 3-2: Schematic and images of water contact angles on solid surfaces corresponding to the two regimes of the spreading coefficient, $S_{os(w)}$, of cyclopentane (o) on a solid (s) in the presence of water (w)

expression for the spreading coefficient is given by Equation 3.1,

$$S_{os(w)} = \gamma_{sw} - \gamma_{os} - \gamma_{wo} \tag{3.1}$$

where, γ is the interfacial tension between the two subscripted phases: solid (s), water (w), and cyclopentane (o). The two regimes of the spreading coefficient of cyclopentane are shown in Figure 3-2.

The positive spreading coefficient of cyclopentane on OTS-treated surfaces indicates the tendency for water to bead up into spherical drops that are extremely mobile on the surface. This may be due to rapid spreading of cyclopentane on OTS in the presence of water, as shown in Figure 3-3. The thin cyclopentane film spreads underneath the water drops and acts as a barrier, limiting the contact area of water and hydrate with the underlying solid. This thin film forms due to the high chemical affinity of OTS terminal groups (-CH_3) to cyclopentane (-CH_2 groups). The -CH_3 group is non-polar (the electronegativity difference between a carbon and hydrogen atom is 0.35 eV and the dipole moment is less than 0.40D) and thus has limited interaction with water. [21] On the other hand, the negative spreading coefficient of cyclopentane

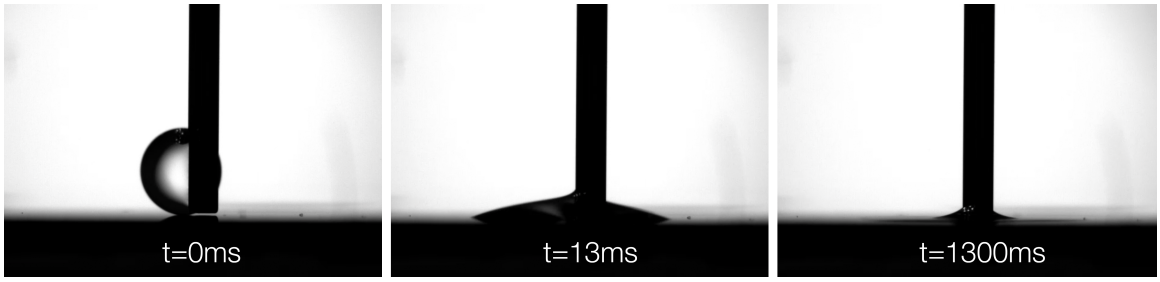

Figure 3-3: Sequence of cyclopentane spreading on an OTS-coated surface in the presence of water

on untreated and FS-treated surfaces results in greater interaction between the solid surface and water and is evident by clear de-pinning of the cyclopentane layer within the water environment. The increased polarity (electronegativity difference 1.78 eV and dipole moment ∼1.51D for C-F bond) of fluorinated groups present on the FS surface is ultimately responsible for the increase in surface-water interaction. Eventually, this leads to greater hydrate formation on untreated and FS-treated surfaces, as shown in Figure 3-1. These effects are not fully captured in the surface energy measurement alone, but are incorporated into the interfacial tensions. Hence we propose using the spreading coefficient as a design parameter for developing hydrate-resistant surfaces.

3.2 Hydrate Growth on Solid Surfaces of Varying Surface Energy

The morphological changes during the formation of a hydrate crystal determine its degree of adhesion to a solid surface. The adhesion strength depends on the surface chemistry and the contact area between the hydrate and the solid surface. Figure 3-4 shows the sequence of the growth of hydrate from a liquid water droplet placed in a cyclopentane bath at 1°C on the three different surfaces used in this work.

On the untreated silicon surface a thin white solid hydrate layer grew outward from the three-phase contact line and eventually covered the entire surface. By expanding beyond the initial contact area, this thin layer is expected to further increase

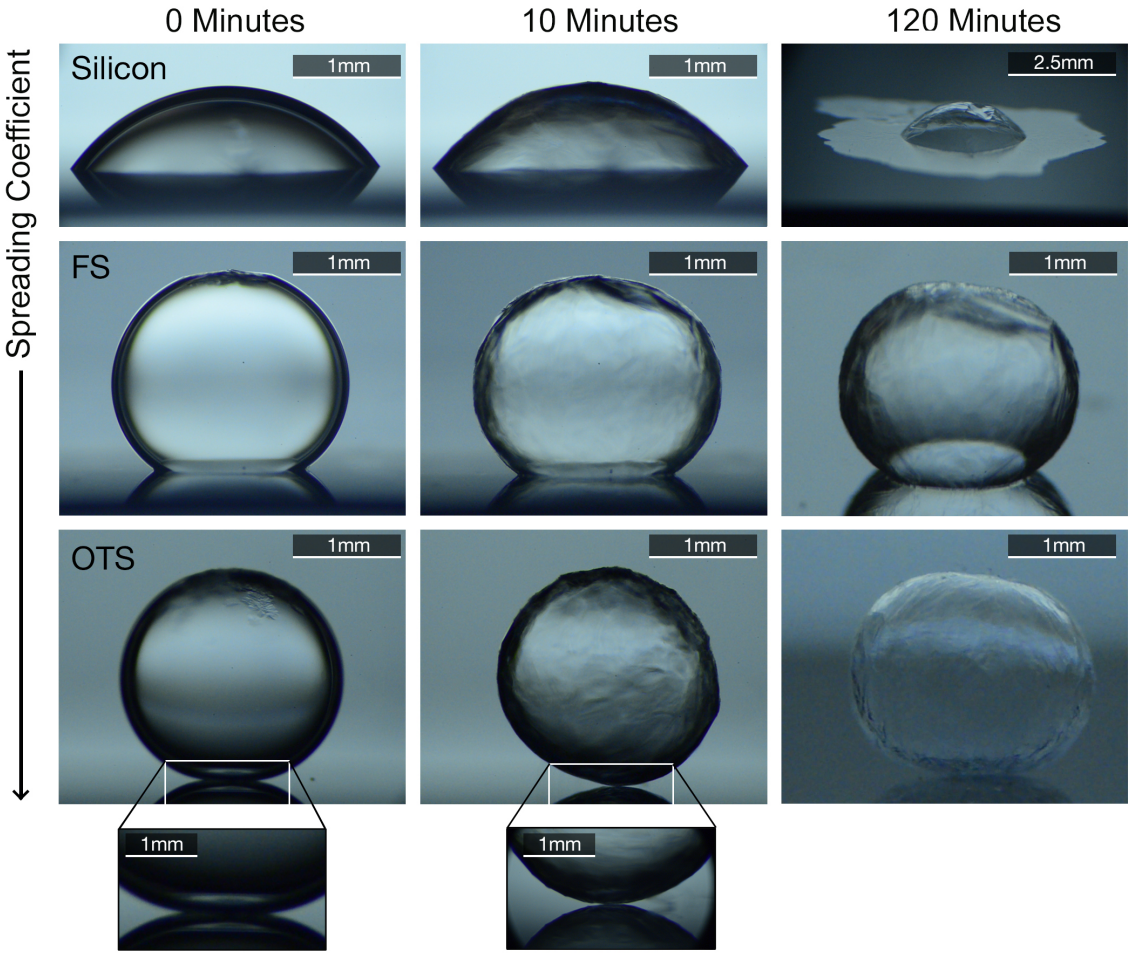

Figure 3-4: Sequences of hydrate growth from chilled water droplets submerged in cyclopentane on surfaces with varied interfacial surface energies.

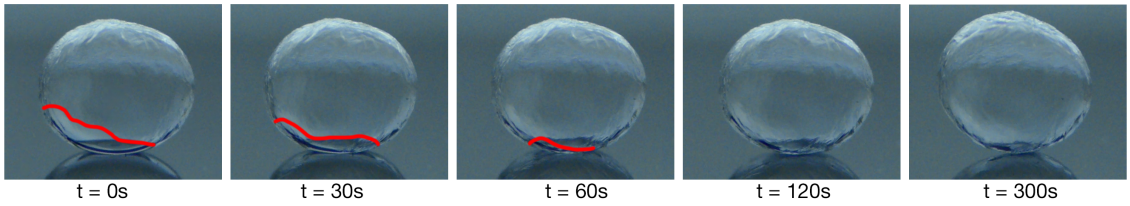

Figure 3-5: Time-lapse of the final formation of hydrate on an OTS-coated surface, with the hydrate front highlighted in red.

the hydrate adhesion to the solid surface. On the other hand, during the hydrate formation on the OTS-coated surface, the interfacial contact area retracts to essentially a single point contact (Figure 3-4 inset). Moreover, during the formation process the droplet was observed to slide and rotate on the OTS-coated surface, as shown in Figure 3-5. As the hydrate formation front initially reaches the solid surface it causes the hydrate to rotate slightly. As additional time passes and the droplet fully transitions to hydrate this rotation increase, which suggests the hydrate has passively detached from the surface. No such changes were observed on the FS-coated surface, and the hydrate maintained the same position and roughly the same contact area as the initial water droplet.

The importance of the contact area and the morphological changes previously observed is emphasized in the surface tilt experiments. After the hydrate crystals nucleated on the surface the solid substrates were gradually tilted from 0° to 90°. At some critical angle, a poorly adhered crystal is expected to slide and fall under its own weight, while strong adhesion would ensure the retention of the hydrate on the surface. Figure 3-6 shows the results of these experiments on untreated, FS-coated and OTS-coated silicon surfaces.

The formation of the thin hydrate layer covering the entire substrate on the untreated silicon surface results in a high adhesion strength such that even a 90° inclination was insufficient for the crystal to detach. On the FS-coated surface, the finite, but lesser, interfacial contact area still resulted in hydrate retention even at a 90° inclination. This is consistent with the absence of a barrier film of cyclopentane on FS and the hydrate crystal being in intimate contact with the solid surface. The

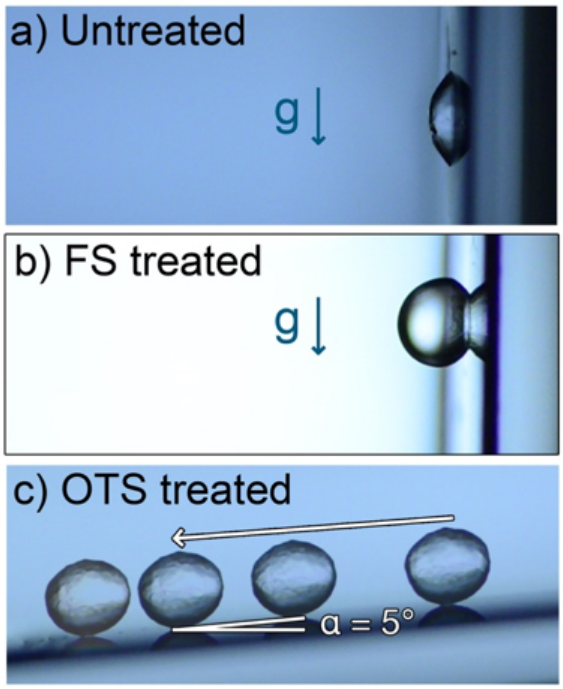

Figure 3-6: Hydrate adheres to (a) untreated silicon and (b) FS-coated silicon up to 90° inclination; movement begins on the (c) OTS-coated silicon at approximately 5° inclination.

OTS-treated surface showed remarkably less adhesion and the hydrate slid off the surface at approximately 5° inclination. The effect of the barrier film of cyclopentane on OTS is supplemented by the morphological changes of the hydrate crystal during its formation resulting in limited contact with the surface (Figure 3-5). This result validates the necessity of the spreading coefficient of cyclopentane to be positive to achieve the lowest possible hydrate adhesion.

3.3 Thermodynamic Stability of Cyclopentane within Rough Surfaces and Hydrate Adhesion

Real surfaces are rarely smooth and the results observed previously have to be extended to rough surfaces for any practical relevance. Here we study the effect of surface roughness on the presence of the cyclopentane barrier film and its wetting properties. We textured each surface using photolithography to obtain square micro-

Table 3.2: Advancing and receding contact angles of cyclopentane in the presence of water

	Advancing angle	Receding angle
Untreated	$125^\circ \pm 3^\circ$	$102^\circ \pm 3^\circ$
FS-treated	$45^\circ \pm 3^\circ$	$13^\circ \pm 1^\circ$
OTS-treated	0°	0°

Table 3.3: Geometric parameters on different textures with $a = 10\mu m$, and $h = 10\mu m$

$b(\mu m)$	ϕ	r	θ_c
5	0.44	2.78	76°
25	0.08	1.33	42°
50	0.03	1.11	26°
75	0.01	1.06	19°

posts with 10μm sides, 10μm depth, and varied spacing between micro-posts. The entrainment of cyclopentane within the surface features underneath the water drop depends on both the surface chemistry and the geometry of the surface texture. For the thermodynamic stability of the entrained film within the surface texture, the contact angle of cyclopentane in the presence of water ($\theta_{os(w)}$) on a smooth surface with the same surface chemistry must be less than a critical angle $\theta_c \equiv cos^{-1}\frac{(1-\phi)}{(r-\phi)}$ where ϕ is the projected solid fraction and r is the roughness ratio. For the samples studied here with square micro-posts of length a, depth h, and spacing b, these parameters are defined as $\phi \equiv \frac{a^2}{(a+b)^2}$ and $r \equiv 1 + \frac{4ah}{(a+b)^2}$. While $\theta_{os(w)}$ depends on the surface chemistry, θ_c is purely a function of the surface geometry. Table 3.2 shows the dynamic contact angles of cyclopentane on different surfaces in water. The values of the critical contact angle θ_c are tabulated in Table 3.3 for the different geometries of the surface texture used here.

When textured surfaces are immersed in a cyclopentane bath with water drops placed on top of them, the surfaces may exist in three different states: an impaled state, an entrained state with the texture tops exposed, and an entrained state with the entire texture submerged (Figure 3-7a). On OTS-treated surfaces, a receding

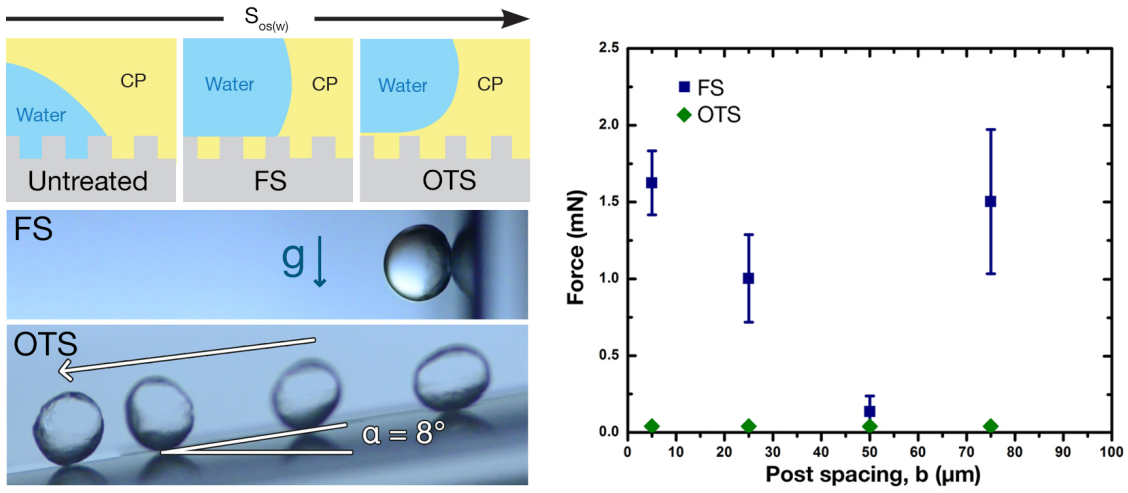

Figure 3-7: (a) Schematic of the thermodynamic states of a textured surface placed in cyclopentane with a water drop on top. (b) Tilt experiments showing hydrate retention on textured FS-treated surfaces even at 90° inclination, while the hydrate moves at 8° tilt on OTS-treated surfaces. (c) Plot of adhesion forces on textured OTS-treated and FS-treated surfaces as a function of the micro-post spacing.

angle of zero indicates successful entrainment of cyclopentane within the surface features ($\theta_{os(w)} < \theta_c$) and submergence of the texture because of the positive spreading coefficient ($S_{os(w)} > 0$). This phenomenon is observed for all geometries, and a barrier film is present to prevent any hydrate stiction. Figure 3-7b validates this hypothesis with the hydrate crystal sliding on the OTS-treated textured surface at a tilt angle of just 8° because of poor adhesion to the surface.

By contrast, the adhesion of hydrate to FS-treated rough surfaces is high. The entrainment of cyclopentane within the surface features depends on the surface geometry of FS-treated surfaces. This entrainment occurs for all surface geometries with $\theta_c > \theta_{os(w)}$, although the texture tops remain exposed to water because of the negative spreading coefficient of cyclopentane. The surface tilt experiments in Figure 3-7b shows the high stiction of the hydrate crystal on FS-treated textured surface even at a 90° tilt angle.

To further quantify the adhesion of hydrate on textured FS-treated and OTS-treated surfaces, a thin steel wire was used as a cantilever to dislodge the hydrates from the surface. The adhesion forces were calculated from the deflection of the

wire and its effective elastic modulus. Hydrate adhesion forces on FS-treated and OTS-treated forces are plotted in Figure 3-7c for different inter-post separations. Textured FS-treated surfaces showed greater adhesion than corresponding textured OTS-treated surfaces, consistent with the results of the surface tilt experiments. The adhesion force on textured FS-treated surfaces initially decreases as inter-post spacing was increased from 5 to 50μm, followed by a sudden increase in adhesion at 75μm. As one may expect, increasing the inter-post spacing decreases the density of micro-posts and reduces the area available for hydrate adhesion. With the tops of the texture of the FS-treated surfaces exposed and possible crystallization of the hydrate into the entrained cyclopentane film, increasing inter-post separation corresponds to decreasing the interfacial contact area. The extent of the hydrate growth into the roughness features of the FS-treated surfaces is still unclear, and further experiments are needed to investigate this thoroughly. For the inter-post spacing of 75μm, as indicated in Tables 3.2 and 3.3, $\theta_{os(w)} > \theta_c$, and cyclopentane is no longer entrained within the texture. This increases the interfacial contact area of water and hydrates to the surface, thereby increasing hydrate adhesion.

OTS-treated surfaces showed about two orders of magnitude lower adhesion than FS-treated surfaces for all the inter-post separations. The highest adhesion strength observed on the texture with 5μm inter-post spacing was approximately 0.02mN. On the textures with greater post separations, hydrates were dislodged without any observed deflection of the steel cantilever, indicating adhesion forces less than 0.004 mN, the lower limit of the experiment.

3.4 Conclusions

The spreading coefficient has been proposed as a predictor of hydrate formation and adhesion in place of conventional surface energy measurements. Smooth and textured silicon samples were treated with either FS or OTS and used to measure hydrate accumulation and adhesion. Despite the significantly lower surface energy of FS-coated surfaces, the OTS-coated samples consistently showed less hydrate accumulation and

almost zero adhesive strength. While surface energy predictions were consistent with the poor performance of untreated silicon, the spreading coefficient of cyclopentane on the solid in water accurately captures the full range of performance across all samples. For a positive spreading coefficient of cyclopentane, the solid-water contact area dramatically shrinks with the formation of a cyclopentane barrier film, which results in greatly reduced hydrate accumulation and adhesion. As such, the OTS-coated samples have shown near-zero accumulation and a two orders of magnitude reduction in adhesion when compared to FS-coated samples. These results suggest that an optimal design of the surface chemistry of the solid surface can promote the formation of a barrier film and provide passive minimization of hydrate accumulation and adhesion.

Chapter 4

Application to Flow Setup

Interfacial phenomena elucidated through static experiments described in Chapter 3 may be more closely expanded to natural systems through the development of a flow-cell setup. Additionally, hydrate formation, especially in industrial applications, is of greatest concern when it impedes fluid flow through a pipe or vessel. As such, a lab-scale flow loop was designed and manufactured to qualitatively assess hydrate formation and adhesion in dynamic, flowing environments; its design is shown schematically and pictorially in Figure 4-1. Design constraints, decisions, and recommendations for the flow loop are the focus of this chapter.

The experimental design consists of four key elements: a chilled fluid reservoir, a chemically-compatible pump system, a data acquisition system (DAQ), and a chilled sample stage. Broadly, these elements must permit the recirculation of the hydrate-forming mixture and detect the formation of initial hydrate crystals, as well as the existence of flow-impeding plugs. Given the propensity to form blockages, components must be designed to withstand increased pressure and safely contain the hydrate-forming mixture; additionally, contamination should be minimized.

4.1 Chilled Fluid Reservoir

The chilled fluid reservoir contains the bulk of the hydrate-forming mixture and should ideally be stored slightly above the hydrate formation temperature (7.7°C for cy-

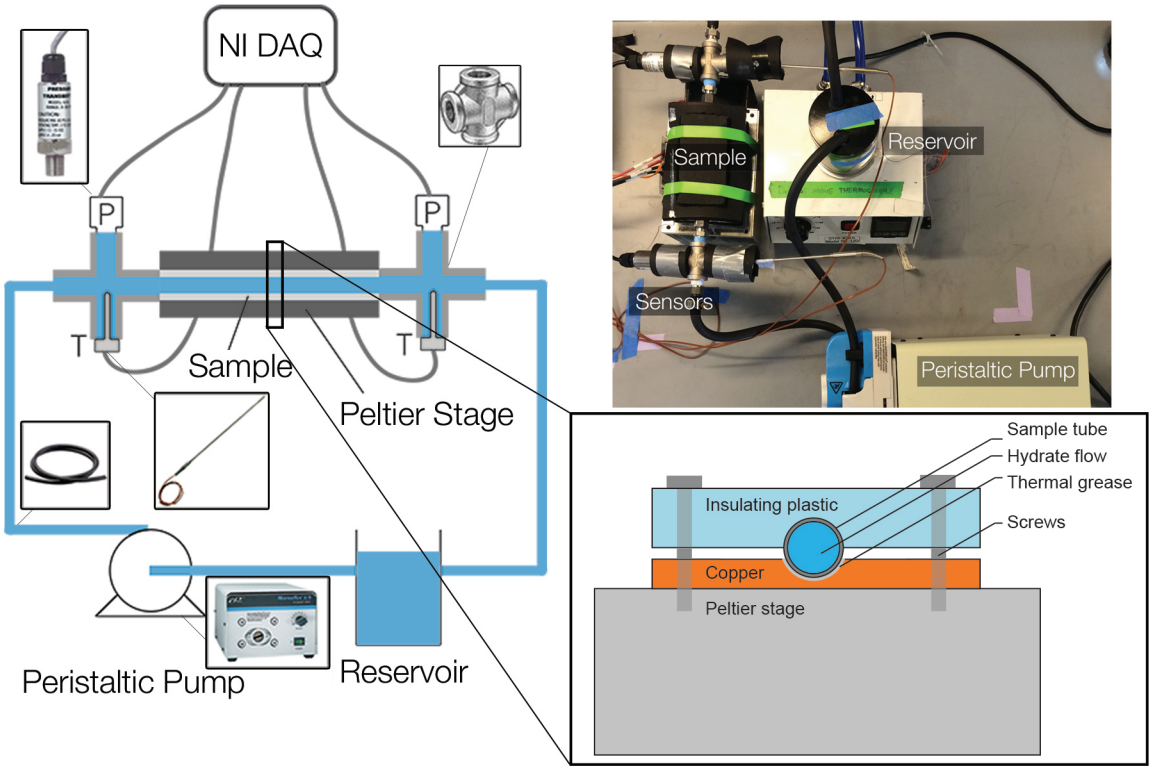

Figure 4-1: Schematic and pictorial representations of a lab-scale flow loop with cross-section of test section

clopentane hydrates). While the warmer temperature constrains hydrate nucleation to the chilled test section, certain experiments may find passing pre-formed hydrates from a sub-cooled reservoir acceptable. Since the flow loop both fills from, and drains into, the reservoir, it should have volume to expand into, and connection with ambient pressure. These constraints ensure that the flow loop piping and test section can be entirely purged of air, and that a vacuum is not formed when initially filling the test section.

When pumping water-cyclopentane mixtures or emulsions, it is desirable to maintain circulation through either a stir bar, externally driven rotor, or sonication, to resist coalescence within the phases. Practically, this may be accomplished with a simple glass jar or beaker placed upon a Peltier stage, such as the Stir-Kool SK-12D (Thermoelectrics Unlimited, Inc.). Glass prevents contamination within the recirculating fluid and may be chemically functionalized, such as with octadecyltrichlorosilane (OTS) to prevent the adhesion or accumulation of hydrate. However, glass is thermally insulating and may limit the temperature range of the reservoir, especially in devices with limited cooling capacity. This may be partially mitigated by using an aluminum or copper reservoir, although care must be exercised to avoid contaminating the hydrate-forming mixture and to prevent excessive hydrate formation in the reservoir.

4.2 Pump System

The pump system provides the driving force for the recirculation of the hydrate-forming mixture and should withstand the harsh environments caused by hydrate formation. Adjustable power or flow-rate enables more expedient testing over a wider range of flow velocities, and corresponding Reynolds numbers. As with the reservoir, care should be exercised to prevent contamination of the hydrate-forming mixture.

Hydrate formation, including the cyclopentane model system, creates a harsh environment for most pumps. Cyclopentane is a strong solvent and may react with the plastic internals of many commercially available pumps. These reactions not

only contaminate the mixture but may also affect pump performance and ultimately destroy the pump. Additionally, creating hydrate plugs inherently blocks the flow throughout the system. Pumping against even a partial blockage may greatly strain most motors and could damage the pump if left unmanaged. Finally, as hydrates begin to form and circulate through the system they may form a slurry with an increased viscosity.

With these constraints, a variable-speed progressive cavity Masterflex L/S peristaltic pump (Cole-Parmer) was selected for the flow loop. The Masterflex pump relies on peristaltic action to squeeze tubing and create a flow. As a result, the pump never comes into contact with the recirculating fluid and eliminates the risk of contamination or reacting with the pump internals. Instead, the pump may act only on insulating, chemically-compatible tubing, such as Viton/Vitube (NewAge Industries). As with most progressive cavity pumps, the Masterflex pump is capable of starting dry (without fluid both immediately upstream and downstream of the device) and is resilient to transient gases passing through. Additionally, the Masterflex pump is relatively unaffected by the increase in viscosity as hydrates begin to form and circulate. However, pumping against an increasing pressure is still a concern and should be eliminated whenever practical. The peristaltic operation also creates a pulsed flow as each cavity progresses into the test section. These pulses may result in transient surges of pressure and could result in some fluid stagnation at low operating speeds.

4.3 Data Acquisition System

The data acquisition records the progression of each experiment and provides indications that hydrates have formed, adhered, and impeded flow. Based on industrial methods of determining hydrate formation, temperatures (with TJ36-CPSS-18U-6 thermocouples, Omega Engineering) and pressures (with Dwyer 626-09-GH-P1-E1-S5 pressure transducers, Instrumart) are measured immediately upstream and downstream of the chilled sample stage. Measurements of the flow temperature provide a metric for the performance of the sample chiller and ensure that the bulk fluid

remains in the hydrate formation window, instead of ice-formation regime. One additional surface thermocouple (SA1-J, Omega Engineering) is placed on the electric Peltier within the chilled sample stage to record the local surface temperature.

Pressure measurements are used to detect the formation of the hydrate, as well as its adhesion to the surface of the test section. An increase in the differential pressure across the test section indicates a blockage is forming within the test section. Should a hydrate plug form in the tubing preceding the test section, pump performance would suffer and circulation may stop, but no pressure change would be recorded. Alternatively, should a hydrate plug form in the tubing proceeding the test section, pressure would build in the entire test section and both pressure transducers would record an increase.

Each component, with the exception of the thermocouple on the Peltier stage, includes only stainless steel wetted surfaces and connects with $\frac{1}{4}$" male NPT threads into a $\frac{1}{4}$" 316 stainless steel pipe cross (4452K482, McMaster). This design decouples the instrumentation and sensors from the physical test section and permits a more rapid sample exchange. Data from the three thermocouples and two pressure transducers is then converted from analog to digital signals and recorded using a National Instruments cDAQ-9174 with a thermocouple card, (NI 9213), analog input card (NI 9215), and LabVIEW software. Data from each sensor is continuously monitored and recorded with a frequency of 0.5Hz.

4.4 Chilled Sample Stage

The chilled sample stage contains the test sample in question and should remain in good thermal contact with the Peltier chiller or other cold source. Shown in Figure 4-1, the cylindrical pipe of interest is secured to the air-cooled Peltier stage (TC-36-25 RS232m, TE Technology, Inc.) through a thermally conductive bottom plate, made of copper, and a thermally insulating upper plate, made of plastic. Each plate comes as a simple slab of material and has a semi-circular slot milled lengthwise across the center axis with a ball end mill corresponding to the diameter of the test

pipe. Thermally conductive paste (76645a14, McMaster) has been applied along the interface between the lower copper block and the test pipe. This paste greatly reduces the interfacial thermal resistance between the two components, which becomes increasingly significant if the exterior of the tube is roughened by a texturing process. While the air-cooled Peltier stage provides sufficient cooling, additional cooling may be sought in the future, and a transition to a water-cooled or oil-cooled jacket may provide additional cooling power.

4.5 Conclusions

As outlined above, the experimental design enables the recirculation of a hydrate-forming mixture with complete chemical compatibility, the ability to detect and monitor the formation of hydrates, and minimal contamination. The recirculating fluid is in contact with surfaces made only of glass, stainless steel, chemically-inert tubing, and the test section. A representative sample of experimental results for untreated and hydrate-repelling surfaces is shown in Figure 4-2 and clearly indicates the onset of hydrate formation, the formation of a solid plug, and strong adhesion once formed.

The upper plot in Figure 4-2 shows the progression of hydrate formation on an untreated surface. As the temperatures of the air-cooled Peltier stage and bulk fluid temperature decrease, a hydrate plug forms and the pump causes a pressure differential between the inlet and outlet sensors. At this point the pump was deactivated to prevent an over-pressure scenario and the Peltier temperature was incrementally increased to 7°C. The pump was subsequently reactivated and the pressure differential continued to rise. Eventually, the Peltier temperature was increased above the dissociation temperature of the hydrate and the pressure was relieved as the hydrate dissociated.

By contrast, the lower plot in Figure 4-2 shows the progression of hydrate formation on a hydrate-repelling surface. As the bulk temperature decreases below 0°C an ice plug is initially formed, but quickly dissociates as the Peltier temperature is increased to 3°C. After approximately 300 seconds at this temperature hydrate begins

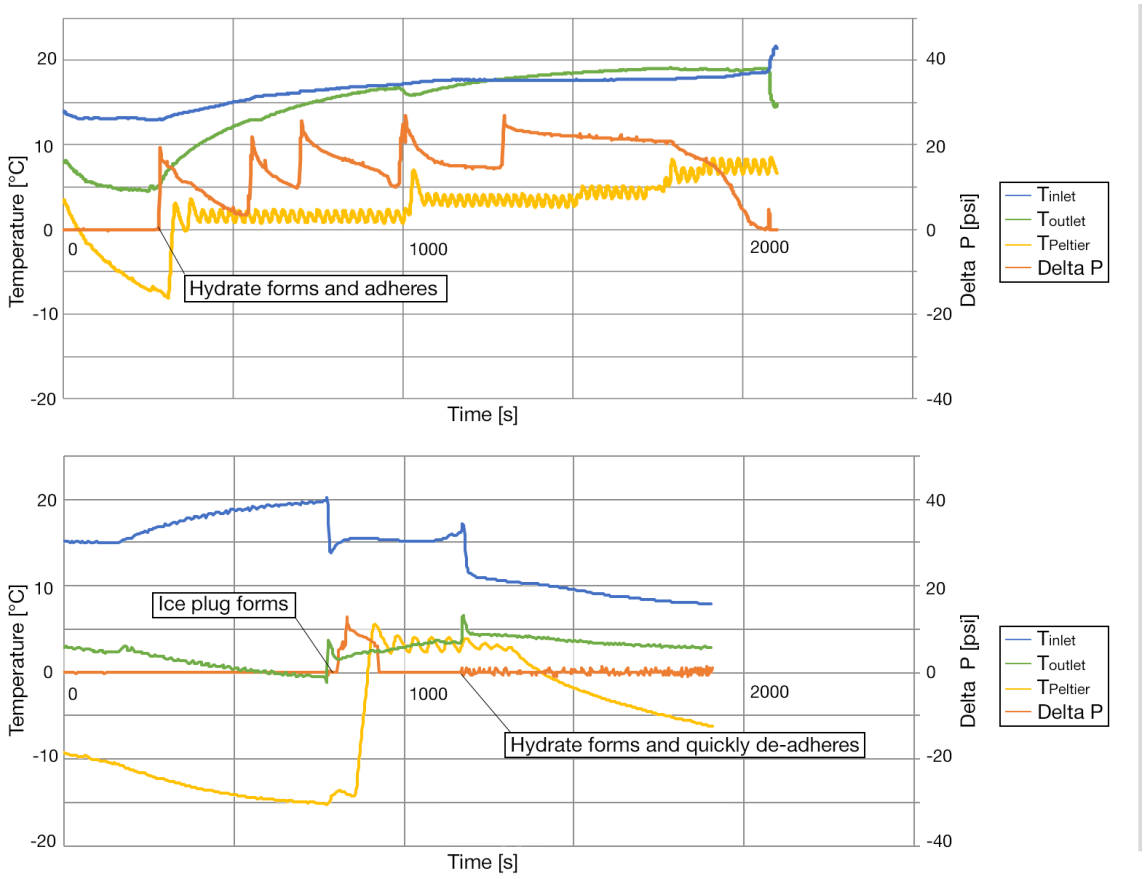

Figure 4-2: Plot of representative data from flow loop experiments on an untreated (above) and hydrate-repelling (below) surface

to form within the test section and introduces small pressure fluctuations across the two pressure gauges. Unlike on the untreated surface, these hydrates are unable to adhere to the walls of the test section and the pressure effect is transient and quickly dissipates.

To conclude, while the static and quasi-static adhesion and accumulation experiments elucidate new insights into the role of the spreading coefficient on hydrate adhesion, both the natural and model systems present new challenges for study under flowing conditions. These challenges manifest as design constraints and limit the practicality or viability of many traditional systems. Nevertheless, design decisions and recommendations have been presented, along with accompanying data on hydrate formation for both hydrate-attracting and hydrate-repelling surfaces. This design may be further expanded and utilized in systematic studies to elucidate additional understandings of the mechanisms for hydrate formation, adhesion, and accumulation within a flowing fluid environment.

Appendix A

LabView Program

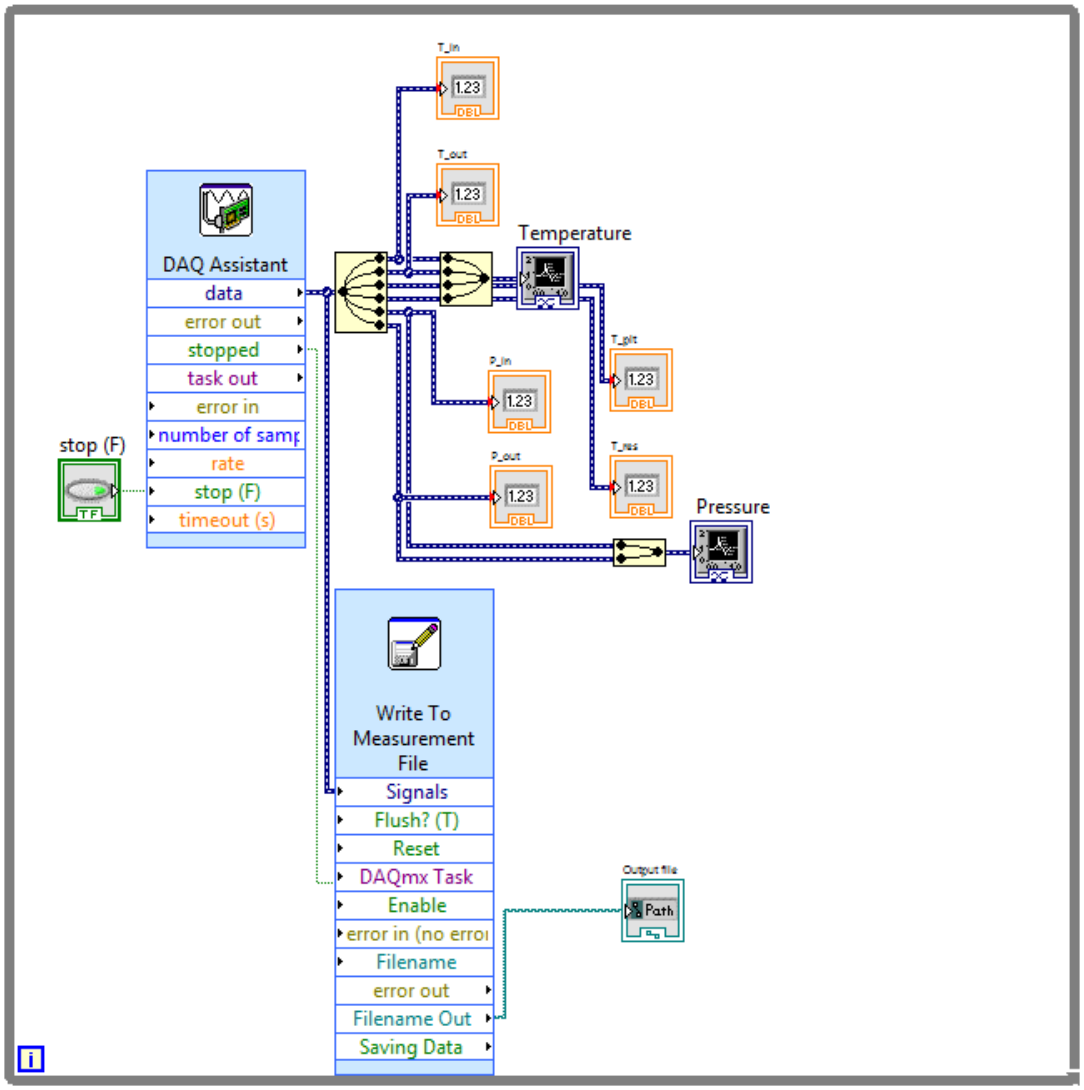

Figure A-1: View of the National Instruments LabVIEW block diagram for flow loop experiments

Bibliography

[1] U.S. Energy Information Administration, *EIA projects world energy consumption will increase 56% by 2040*, Web. <http://www.eia.gov/todayinenergy/detail.cfm?id=12251> (2016).

[2] E. D. Sloan, C. A. Koh, *Clathrate Hydrates of Natural Gases*, CRC Press, Boca Raton (2007).

[3] A. K. Sum, C. A. Koh, E. D. Sloan, *Ind. Eng. Chem. Res.* **48**, 7457 (2009).

[4] R. Pallardy, *Deepwater Horizon oil spill of 2010*, Web. <http://www.britannica.com/event/Deepwater-Horizon-oil-spill-of-2010> (2016).

[5] K. A. Kvenvolden, *Chemical Geology* **71**, 41 (1988).

[6] B. C. Gbaruko, J. C. Igwe, P. N. Gbaruko, R. C. Nwokeoma, *J. Petroleum Sci. and Eng.* **56**, 192 (2007).

[7] C. A. Koh, R. E. Westacott, W. Zhang, K. Hirachand, J. L. Creek, A. K. Soper, *Fluid Phase Equilibria* **194**, 143 (2002).

[8] E. D. Sloan Jr, *Nature* **426**, 353 (2003).

[9] J. W. Nicholas, L. E. Dieker, E. D. Sloan, C. A. Koh, *J. Colloid Interface Sci.* **331**, 322 (2009).

[10] G. Aspenes, L. E. Dieker, Z. M. Aman, S. Høiland, A. K. Sum, C. A. Koh, E. D. Sloan, *J. Colloid Interface Sci.* **343**, 529 (2010).

[11] Z. M. Aman, L. E. Dieker, G. Aspenes, A. K. Sum, E. D. Sloan, C. A. Koh, *Energy & Fuels* **24**, 5441 (2010).

[12] Z. M. Aman, E. P. Brown, E. D. Sloan, A. K. Sum, C. A. Koh, *Phys. Chem. Chem. Phys.* **13**, 19796 (2011).

[13] J. D. Smith, A. J. Meuler, H. L. Bralower, R. Venkatesan, S. Subramanian, R. E. Cohen, G. H. McKinley, K. K. Varanasi, *Phys. Chem. Chem. Phys.* **14**, 6013 (2012).

[14] Z. M. Aman, W. J. Leith, G. A. Grasso, E. D. Sloan, A. K. Sum, C. A. Koh, *Langmuir* **29**, 15551 (2013).

[15] Z. M. Aman, E. D. Sloan, A. K. Sum, C. A. Koh, *Phys. Chem. Chem. Phys.* **16**, 25121 (2014).

[16] W. Lee, S. Baek, J.-D. Kim, J. W. Lee, *Energy & Fuels* **29**, 4245 (2015).

[17] H. Sojoudi, M. R. Walsh, K. K. Gleason, G. H. McKinley, *Langmuir* **31**, 6186 (2015).

[18] S. A. Morrissy, V. W. Lim, E. F. May, M. L. Johns, Z. M. Aman, B. F. Graham, *Energy & Fuels* **29**, 6277 (2015).

[19] P. U. Karanjkar, J. W. Lee, J. F. Morris, *Cryst. Growth Des.* **12**, 3817 (2012).

[20] J. D. Smith, R. Dhiman, S. Anand, E. Reza-Garduno, R. E. Cohen, G. H. McKinley, K. K. Varanasi, *Soft Matter* **9**, 1772 (2013).

[21] J. E. Huheey, *Inorganic Chemistry: Principles of Structure and Reactivity, 2nd Ed.*, Harper and Row (1978).